ADVANCED FUNCTIONAL MATERIALS
www.afm-journal.de

Leaf-like Graphene Oxide with a Carbon Nanotube Midrib and Its Application in Energy Storage Devices

Ziyang Guo, Jie Wang, Fei Wang, DanDan Zhou, Yongyao Xia, and Yonggang Wang**

Graphene oxide (GO) has recently attracted a great deal of attention because of its heterogeneous chemical and electronic structures and its consequent exhibition of a wide range of potential applications, such as plastic electronics, optical materials, solar cells, and biosensors. However, its insulating nature also limits its application in some electronic and energy storage devices. In order to further widen the applications of GO, it is necessary to keep its inherent characteristics while improving its conductivity. Here, a novel leaf-like GO with a carbon nanotube (CNT) midrib is developed using vapor growth carbon fiber (VGCF) through the conventional Hummers method. The CNT midrib provides a natural electron diffusion path for the leaf-like GO, and therefore, this leaf-like GO with a CNT midrib displays excellent performance when applied in energy storage devices, including Li-O_2 batteries, Li-ion batteries, and supercapacitors.

1. Introduction

Graphene oxide (GO) is an atomically thin sheet of graphite containing saturated sp^3 carbon atoms bound to oxygen on their basal planes and edges; it can be considered a precursor for graphene synthesis by either chemical or thermal reduction processes.[1–3] It is currently attracting more and more attention because of its heterogeneous chemical and electronic structures.[1–12] The polar oxygen functional groups result in the good dispersibility of GO in many solvents, which is quite important for processing and further derivatization. In addition, these functional groups serve as sites for chemical modification or functionalization of GO, which in turn can be employed to immobilize various active species through covalent or noncovalent bonds. On the other hand, GO is an electronic hybrid material that features both conducting π-states from sp^2 carbon sites and a large energy gap (carrier transport gap) between the σ-states of its sp^3-bonded carbons. The tunability of the ratio of the sp^2 and sp^3 fractions by reduction is a powerful way to tune its bandgap and therefore controllably transform GO from an insulator to a semiconductor and to a graphene-like semi-metal.[6] Accordingly, GO displays a wide landscape of applications ranging from plastic electronics, optical materials and solar cells, to biosensors.[1–13] However, the insulating nature of GO also limits its application in some electronic devices and energy storage devices. Although chemical or thermal reduction can effectively improve its electronic conductivity, the inherent characteristics of GO resulting from these oxygen functional groups are also consumed. Furthermore, residual defects and holes still limit the electronic quality of reduced GO.[6,14] Therefore, the best way to further widen the application of GO is to keep its inherent characteristics while improving its conductivity.

Herein, we develop a novel leaf-like GO with a carbon nanotube (CNT) midrib by a facile method. The CNT midrib provides a natural electron diffusion path for the GO leaf. Thus, this leaf-like GO with a CNT midrib displays excellent performance when applied in Li-O_2 batteries. In addition, it also exhibits promising applications in other energy storage devices, such as Li-ion batteries and supercapacitors.

2. Character of Leaf-like GO

In our strategy (**Figure 1**), vapor growth carbon fiber (VGCF) was used as the carbon source for GO synthesis by the conventional Hummers method.[15] The structure characteristic of the applied VGCF can be roughly (or approximately) summarized as: multi-layered graphene (or multi-layered graphite structure) wound around a CNT axis to form a hollow graphite rod (Figure 1a, Figure S1 in the Supporting Information, and the corresponding discussions). By Hummers method, the multi-layered graphene is extended along with the CNT axis, and the multi-layered graphene is exfoliated to form less-layered GO (Figure 1b). Finally, VGCF is converted into the leaf-like GO with a CNT midrib (Figure 1c).

Figure 2 shows transmission electron microscope (TEM) images of the applied VGCF with different magnifications. It can be detected from Figure 2a that the VGCF exhibits the structure of hollow rod. The VGCF is typically around 150 nm in diameter, and can be up to several μm in length. The TEM image of the top of VGCF, shown in Figure 2b, further confirms its hollow structure which consists of a spiral multi-layered graphene (Figure 2c and Figure S1 in the Supporting Information). Figure 2d shows a high-resolution TEM (HRTEM)

Dr. Z. Y. Guo, Dr. J. Wang, Dr. F. Wang, Dr. D. D. Zhou, Prof. Y. Y. Xia, Prof. Y. G. Wang
Department of Chemistry and Shanghai Key Laboratory of Molecular Catalysis and Innovative Materials, Institute of New Energy
Fudan University
Shanghai 200433, China
E-mail: yyxia@fudan.edu.cn; ygwang@fudan.edu.cn

DOI: 10.1002/adfm.201300130

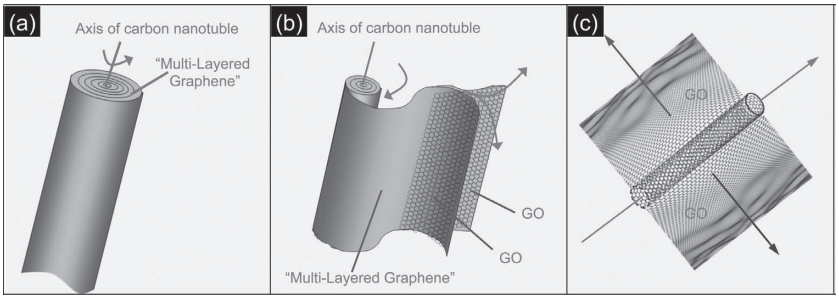

Figure 1. Schematic illustration of the preparation process (from pristine VGCF to the product of leaf-like GO with a carbon nanotube midrib).

image of the multi-layered graphene; it can be observed that the layer-number of multi-layered graphene is in the range 3 to 7 (Figure 2d). The as-prepared sample from VGCF by Hummers method was also characterized by TEM for comparison (**Figure 3**). As shown in Figure 3a, the raw material of VGCF has been converted into layered GO with a CNT axis that is the residual center axis of VGCF. The HRTEM image (Figure 3b) further confirms the residual center axis of VGCF is a typical CNT with an outer diameter of 20 nm and an inter diameter of 5 nm. The outer diameter of the CNT is much smaller than that of pristine VGCF, indicating that the spiral structure (Figure 2) has been opened along with the CNT axis. These TEM images (Figure 3c–e) further demonstrate that all of these as-prepared GO have the same structure characteristic, and can be summarized as the leaf-like GO with a CNT midrib. The SEM images of the as prepared leaf-like GO are given in Figure S2 (Supporting Information).

The powder X-ray diffraction (XRD) pattern of as-prepared leaf-like GO is shown in **Figure 4**a, where it is compared with that of pristine VGCF. The diffraction peaks of VGCF at around 26.2°, 42.8°, 53.8°, and 77.8° are attributed to the (002), (100), (004), and (110) diffraction peaks of graphite [JCPDS: PDF 75-1621], respectively.[16] The (002) diffraction peak of leaf-like GO is wider and much less intense than that of VGCF because the graphite structure is exfoliated by Hummer method. The (001) diffraction peak of as-prepared leaf-like GO can be observed as around 10.9°, corresponding to a typical d -spacing of 0.81 Å.[3] The leaf-like GO was also investigated by Raman spectroscopy (Figure 4b). The spectra are characterized by two prominent peaks at 1330 and 1574 cm^{-1}, which correspond to the D and G modes, respectively.[17,18] The G-band corresponds to the first-order scattering from the doubly degenerate E_{2g} phonon modes of graphite at the Brillouin zone center and is characteristic of all sp^2-hybridized carbon networks; the dispersive D-band arises from phonon branches within the interior of the graphite Brillouin zone that is activated by scattering from defects;[17,18] the I_D/I_G ratio provides a sensitive measure of the disorder and crystallite size of the graphitic layers. The I_D/I_G ratio of leaf-like GO is much higher than that of pristine VGCF (Figure S3 in the Supporting Information). Additionally, another prominent second-order dispersive feature, the D′-band, is observed at around 2660 cm^{-1} and is thought to originate from a two-phonon double resonance process.[17,18] High-resolution C1s X-ray photoelectron (XPS) spectra of leaf-like GO are given in Figure 4c. The sp^2 peak of the C1s envelope centers at 284.5 eV.[19] The component at 286.03 eV is assigned to C atoms directly bonded to oxygen in hydroxyl configurations (C–O). The smaller components at 287.37 and 288.89 eV are related to carbonyl (C=O) and carboxyl groups (COOH or HO–C=O). XPS spectra of as-prepared leaf-like GO are given in Figure S4 (Supporting Information). The Fourier transform-infrared spectrophotometer (FT-IR) spectrum of leaf-like GO (Figure 4d) illustrates peaks corresponding to C–O (carbonyl) at 1050 cm^{-1}, the C–O–C epoxy group at ca. 1250 cm^{-1}, and carboxyl-associated O–H at ca. 1413 cm^{-1}.[20–22] The peak at ca. 1600 cm^{-1} is identified as arising from C–C vibrations of the graphitic domains.[20–22] A C=O peak from carboxylic acid is observed at 1728 cm^{-1}.[20–22] The relatively broad peak at 3360 cm^{-1} could be due to the adsorbed water on the surface of the GO.[20–22] The BET surface area of the resulting material was measured to be 200.8 $m^2\ g^{-1}$.

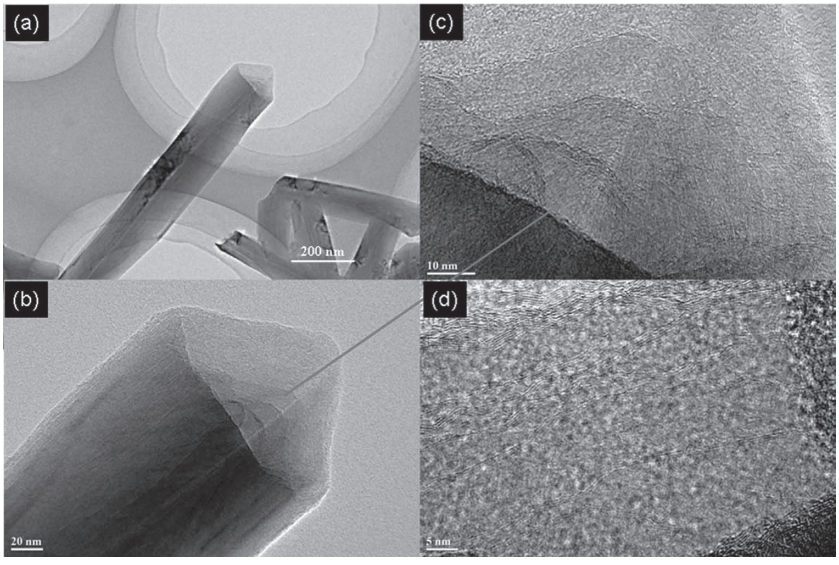

Figure 2. TEM images of pristine VGCF at various magnifications.

In theory, GO should be a very promising electrode active material for energy storage devices, because the good dispersibility and two-dimensional structure of GO can result in very uniform electrolyte/electrode interface. However, owing to the inherent insulating nature, conventional GO cannot be used as the active site for any electrochemical reaction. However, this drawback does not exist for leaf-like GO. As shown in Figure 3, the CNT can be considered as a natural electron diffusion midrib for the leaf-like GO. The electronic conductivities of the leaf-like GO powder, conventional GO powder prepared by Hummers method

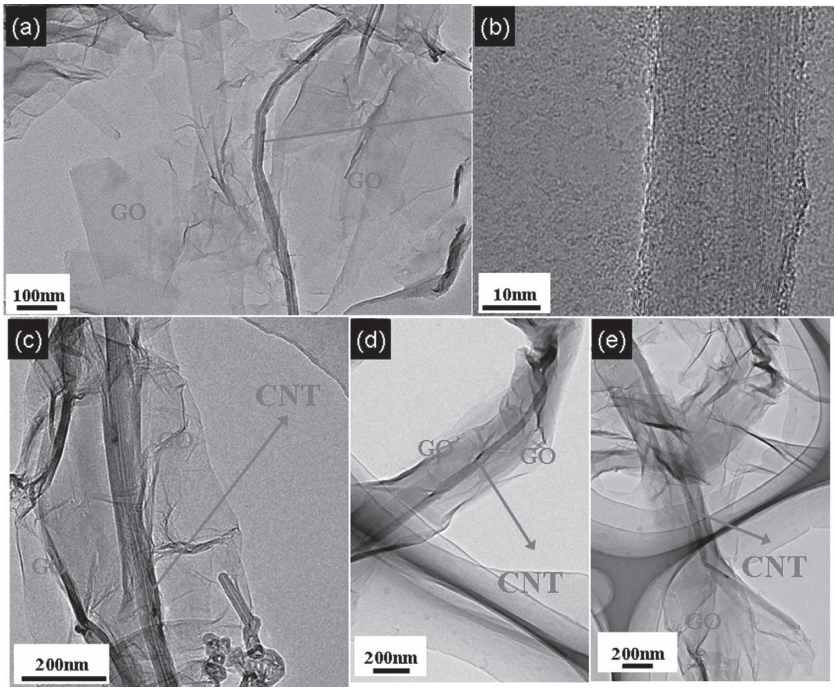

Figure 3. TEM images of as-prepared leaf-like GO with a carbon nanotube midrib at various magnifications.

from graphite, and commercial CNT powder (Nanotech Port CO., Ltd, Shenzhen, China) were investigated at a pressure of 4 MPa by a four-pole conductivity instrument for power materials.

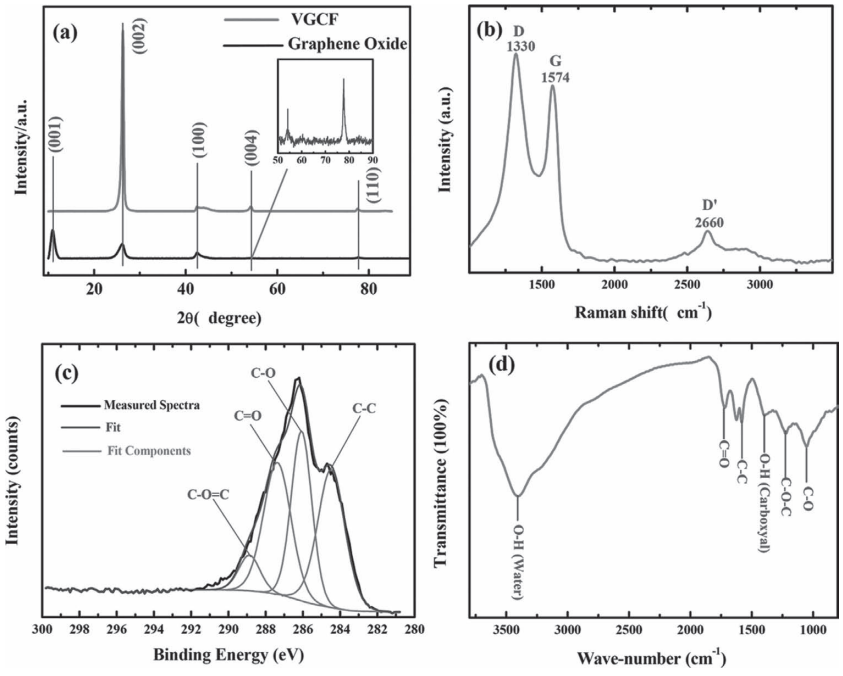

Figure 4. Characterization of as-prepared leaf-like GO: a) XRD patterns of pristine VGCF and leaf-like GO; b) Raman spectra of leaf-like GO; c)high-resolution C1*s* XPS spectra of leaf-like GO; and d) FT-IR transmittance spectra of leaf-like GO.

As shown in **Table 1**, the electronic conductivity of leaf-like GO powder is close to that of CNT powder, and is much higher than that of conventional GO powder. Therefore, the leaf-like GO becomes the active site for various electrochemical reactions (e.g., O_2 reduction, Li intercalation, and ion adsorption/desorption), and can be applied in different energy storage devices. In this, the as-prepared leaf-like GO was mainly applied as electrode material for Li-O_2 batteries. Its other potential applications in Li-ion batteries and supercapacitors are briefly introduced.

3. Application in Rechargeable Li-O_2 Batteries

In the investigation of Li-O_2 battery, leaf-like GO was used as the active material for O_2 catalytic electrode. The Li-O_2 battery, containing a leaf-like GO-based O_2 catalytic electrode (positive) and a Li-electrode (negative) in a tetra(ethylene) glycol dimethyl ether–lithium triflate ($TEGDME–LiCF_3SO_3$) electrolyte,[23] was constructed as described in the methods section and Supporting Information. As shown in **Figure** 5a, when applied with a low current density of 50 mA g^{-1}, the leaf-like GO-based Li-O_2 battery can display a high discharge capacity of 6000 mA h g_{GO}^{-1} (or 6 mA h cm^{-2} calculated based on the geometric area of O_2 catalytic electrode and 2.98 A h cm^{-2} calculated based on the BET surface area of leaf-like GO in O_2 catalytic electrode) with a cut-off voltage of 2.0 V. The electrode reactions on discharge/charge can be summarized as:[23]

$$O_2 + 2Li^+ + 2e^- \longrightarrow Li_2O_2 \quad (1)$$

According to Equation (1), O_2 is reduced into Li_2O_2 on discharge. The charge process reverses the discharge process. In order to clarify this operating mechanism, ex situ XRD analysis (Figure 5b) was conducted, in sequence, on the leaf-like GO-based Li-O_2 battery in its pristine state (XRD1), after full discharge for formation of Li_2O_2 (XRD2), and after complete recharge for the reconversion of Li_2O_2 (XRD3).[23] It can be seen from Figure 5b that the characteristic peaks related to Li_2O_2 exist in the XRD2 discharge patterns and vanish again in the XRD3 charge patterns. These results well support the interpretation about the operating mechanism of Li-O_2 battery, and also quite agree with Jung et al.'s recent report about the Li-O_2 battery using carbon material as catalyst.[23] Figure 5c presents typical voltage profiles for the leaf-like GO-based Li-O_2 battery

Table 1. Electronic conductivities of leaf-like GO, conventional GO, and CNT powders measured at a pressure of 4 MPa.

Material	Leaf-like GO powder	GO powder	CNT powder
Conductivity [S cm^{-1}]	0.7	8×10^{-5}	35.0

cycled at a current density of 200 mA g^{-1} and at a fixed capacity of 1000 mA h g_{GO}^{-1}.[23] As shown in Figure 5c, the operating voltage and capacity of battery is quite stable over 150 cycles, indicating the excellent stability of leaf-like GO for O_2 catalytic reduction. Obviously, this result also demonstrates the good stability of the TEGDME–$LiCF_3SO_3$ electrolyte in the operation of the Li-O_2 battery.[23] Recently, the rechargeable non-aqueous Li-O_2 battery has received a great deal of interest because theoretically its specific energy far exceeds the best that can be achieved with Li-ion batteries.[23–28] However, poor cycle life is the greatest challenge for this technology.[25] Only very recently, it was reported that Li-O_2 batteries can realize 100 cycles.[23,24] Polarization behavior may arise between the 100th and 150th cycles due to drying of electrolyte over the long charge/discharge cycle, which results in the reduction of liquid–solid–gas three-phase interface area; in this situation, the Li_2O_2/O_2 conversion is not totally reversible. The remnant discharge product may incrementally clog the porous electrode, so resulting in the polarization behavior. Furthermore, drying of the electrolyte may also increase the internal resistance, increasing polarization. Thereby, for building long-cycle Li-O_2 batteries, it is also necessary to reduce the evaporation of electrolyte because the Li-O_2 battery is an open system. In order to further demonstrate the advantages of leaf-like GO for Li-O_2 batteries, conventional GO prepared by Hummers method from graphite, commercial CNTs (Nanotech Port Co., Ltd, Shenzhen, China), and their direct mixture (GO/CNT weight ratio: 1:1) were employed as the catalysts for Li-O_2 batteries. Their discharge/charge curves within the potential window between 2.0 and 4.5 V at a current density of 50 mA g^{-1} are given in Figure 5d for comparison. Their achieved discharge capacities are 2250 mA g_{GO}^{-1} (conventional GO-based Li-O_2 battery), 2500 mA g_{CNT}^{-1} (CNT-based Li-O_2 battery), and 3000 mA $g_{CNT/GO}^{-1}$(CNT/GO mixture-based Li-O_2 battery). Obviously, these achieved capacities are much lower than that of leaf-like GO-based Li-O_2 battery. One reason is that the electronic conductivity of leaf-like GO powder (0.7 S cm^{-1}) is close to that of CNT powder (35 S cm^{-1}), and is much higher than that of conventional GO powder (8×10^{-5} S cm^{-1}) (see Table 1). It is more important that in leaf-like GO the CNT can be considered as a natural electron diffusion midrib for the leaf-like GO, which makes the leaf-like GO have more active sites for O_2 reduction reaction (**Figure 6**). Although the conventional GO prepared by Hummers method from graphite has a large surface area, its inherent low electronic conductivity much limits the electrons transfer. Only very limited regions of GO, which directly obtains electrons from the current collector, can be utilized as the active sites for O_2 reduction (Figure 6a). For CNT, the high electronic conductivity facilitates the transfer of electrons (Figure 6b). However, its surface area is not very high (especially, the inner surface of CNT can not be utilized for O_2 reduction). In theory, the mixture of CNT/GO can unite the advantages of CNT and GO. However, in practice, the CNT cannot be uniformly connected with the layered GO (Figure 6c), which still limits the active sites for O_2 reduction. The leaf-like GO effectively unites the advantages from CNT and GO. As shown in Figure 6d, the CNT provides a natural electron diffusion midrib for the leaf-like GO, which makes the leaf-like GO have more active sites for O_2 reduction reaction.

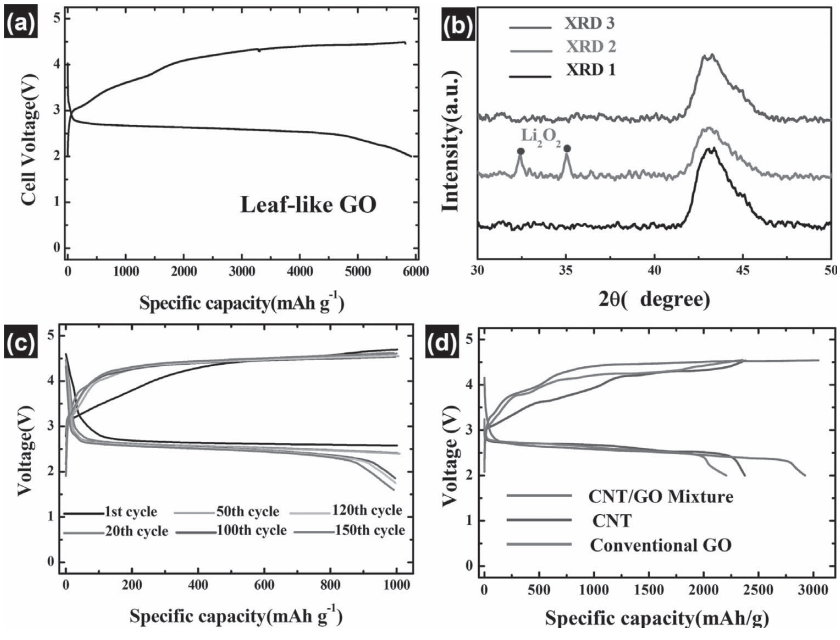

Figure 5. a) Discharge/charge curves of an Li-O_2 battery using leaf-like GO as catalyst at a low current density of 50 mA g^{-1} within the voltage window between 2.0 and 4.5 V. b) Sequence of ex situ XRD analysis carried out on the leaf-like GO-based Li-O_2 battery in its pristine state (XRD1), after full discharge (XRD2), and after full charge (XRD3). c) Cycle performance of Li-O_2 battery using leaf-like GO as catalyst at a current density of 200 mAg^{-1} with a fixed capacity of 1 000 mA h g_{GO}^{-1}. d) Discharge/charge curves of Li-O_2 batteries using conventional GO, CNTs, and a GO/CNT mixture as catalysts at a current density of 50 mA g^{-1} within the voltage window between 2.0 and 4.5 V.

4. Application in Li-Ion Batteries

In recent years, various carbon materials have been widely applied as the buffer matrix for some electrode active materials (e.g., Si, Sn, metal oxides, etc.) of Li-ion batteries to compensate for the expansion of the reactants on Li-intercalation, so preserving particle contact essential for charge transmission.[29–32] Here, the mixture of leaf-like GO and Si nanoparticles (weight ration of GO/Si is 3:7) was employed as the anode for a Li-ion battery (see the Experimental Section for

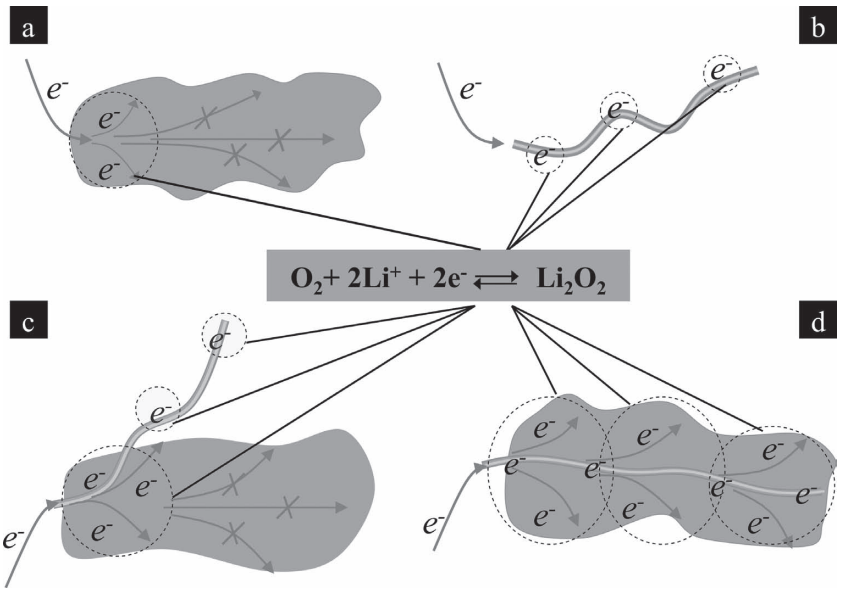

Figure 6. Schematic illustrations of electrons transfer on: a) conventional GO, b) CNTs, c) GO/CNT mixture, and d) leaf-like GO.

detail). This cell was cycled within the potential window from 2.0 to 0 V (vs. Li/Li^+) with a current density of 200 mA g^{-1}. As shown in **Figure 7**a, the capacity loss of the GO/Si composite electrode is almost negligible over 100 cycles, indicating high cycling performance. This result can demonstrate that the as-prepared GO is a promising buffer material for Si electrode. Figure 7b gives discharge/charge curves at the selected cycle number (1st, 10th, 50th, and 100th). It can be observed that the leaf-like GO/Si composite electrode displays obvious irreversible capacity on initial discharge/charge cycle with a cut-off charge potential of 2 V. This is because that the SEI film formation (i.e., reduction of electrolyte) provides irreversible capacity on initial discharge. In addition, the large surface area (200 m^2 g^{-1}) of leaf-like GO further increases the undesired SEI film formation, which also aggravates the irreversibility of leaf-like GO/Si composite electrode on initial discharge. Furthermore, the surface groups on leaf-like GO definitely also participate in the side reactions during the first discharge (Figure 7c). As shown Figure 7c, the pure leaf-like GO displays a large capacity of about 1500 mA h g^{-1} on initial discharge. However, its charge process only releases a reversible charge capacity of about 400 mA h g^{-1}. In other words, although leaf-like GO is a promising buffer material for Si electrode, its large surface area and surface groups also much aggravate the irreversibility of leaf-like GO/Si composite electrode on initial cycling. On the other hand, the achieved reversible capacity of leaf-like GO/Si composite is still lower than the theoretical capacity of Si (4200 mA h g^{-1} × 70%; the weight ration in the composite of GO/Si is 3:7). Generally, increasing the wt% of carbon additive or reducing test current density can further increase the utilization of Si. When we further reduce the test current to 50 mA g^{-1}, the leaf-like GO/Si composite electrode delivers a maximum reversible capacity of ca. 1900 mA g^{-1} (Figure 7d).

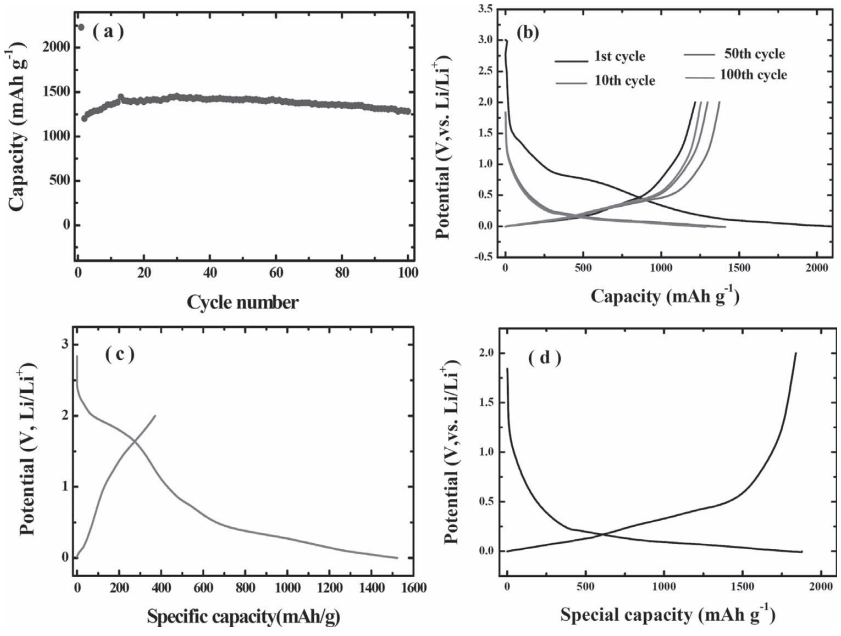

Figure 7. a) Cycle performance (discharge capacity vs. cycle number) of leaf-like GO/Si composite electrode at a current density of 200 mA g^{-1}. b) Discharge/charge curves of leaf-like GO/Si composite electrode at different cycle numbers. c) Initial discharge/charge cycle of pure leaf-like GO at a current density of 200 mA g^{-1} with a cutoff potential of 2 V on charge. d) Discharge/charge curves of leaf-like GO/Si composite electrode a low current density of 50 mA g^{-1}.

5. Application in Supercapacitors

Finally, the as-prepared leaf-like GO was also used as the electrode active material for supercapacitors or electrical double-layer capacitors (EDLC). The preparation of leaf-like GO-based electrode and assembly of EDLC are described in the Experimental section. Cyclic voltammetry (CV) curves of the leaf-like GO-based are shown in **Figure 8**a. As show in Figure 8a, the CV curves of GO-based EDLC display a rectangular shape, indicating a typical capacitance characteristic.[33,34] It can be observed that the special capacitance of leaf-like GO is 6.2 μF cm^{-2} at a sweep rate of 50 mV s^{-1}. Even at the very high sweep rate of 20 000 mV s^{-1}, the capacitance of leaf-like GO is still as high as 2.5 μF cm^2. This result clearly demonstrates the ultra-fast charge/discharge ability of leaf-like GO. The capacitance was calculated according to:

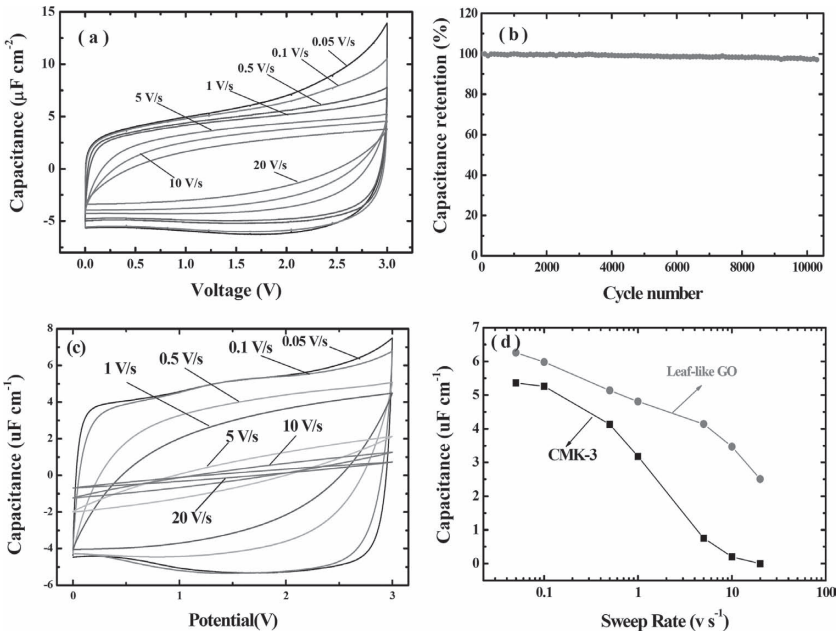

Figure 8. a) CV curves of leaf-like GO based EDLC with different sweep rates. b) Cycle life of leaf-like GO-based EDLC tested with a sweep rate of 5 V s^{-1}. c) CV curves of CMK-3 based EDLC with different sweep rates. d) Power performance (capacitance vs. sweep rate) comparison between leaf-like GO-based EDLC and CMK-3 based EDLC.

$$C = \frac{I}{vs} \tag{2}$$

where I is the current intensity (A) at 1.5 V observed on the negative sweep process of the CV test; v is the sweep rate (V s^{-1}); s is the surface area of active materials (cm^2), calculated as [active materials mass loading in an electrode (g)] × [BET surface area of active materials (cm^2 g^{-1})]. Figure 8b gives the cycle performance of leaf-like GO based EDLC, indicating perfect cycling ability. It has been reported[35–39] that ordered mesoporous carbons with a narrow distribution in the mesopore range and a uniform pore connection have much better electrochemical capacitance performance than conventional carbon materials, due to the mesopore channels and interconnections providing a more favorable path for penetration and transportation of ions. In order to emphasize the advantage of leaf-like GO for the application in EDLC, we thereby compared the electrochemical capacitance performance of ordered mesoporous carbon (CMK-3) with that of leaf-like GO. In this experiment, ordered mesoporous carbon CMK-3 (pore-size: 3 to 5 nm, BET: 1431 m^2 g^{-1}, produced by XF Nano, INC, China) was used as received. The preparation of the CMK-3 based EDLC was the same as that of leaf-like GO-based EDLC. As shown in Figure 8c, CV curves of CMK-3 based EDLC only display the rectangular shape at low sweep rates (from 0.05 to 1 V s^{-1}). However, the leaf-like GO-based EDLC can retain the rectangular shape of CV at a high sweep rate of 20 V s^{-1}. It can also be observed from Figure 8d that the power performance (capacitance vs. sweep rate) of leaf-like GO based EDLC is much higher than that of CMK-3 based EDLC. It is assumed that these oxygen groups and the two-dimensional structure make the leaf-like GO be well wetted by electrolyte, and thus reduce interface resistance and improve the rate performance of EDLC. In addition, the high electronic conductivity (0.7 S cm^{-1}) can also reduce the internal resistance of the electrode.

6. Conclusions

A novel leaf-like GO with a CNT midrib was prepared from VGCF through the conventional Hummers method. The CNT midrib provides a natural electron diffusion path for the GO leaf. This kind of GO displays excellent performance when applied in Li-O_2 batteries. Furthermore, it also exhibits promising applications in Li-ion batteries and supercapacitors.

7. Experimental Section

Preparation and Characterization: Leaf-like GO was synthesized from VGCF (provided by Showa Giken Industrial Co., Ltd, Japan) by the method of Hummers. The pristine VGCF (2 g) was put into cold (0 °C) concentrated H_2SO_4 (46 mL) solution containing 1 g $NaNO_3$. $KMnO_4$ (6 g) was added gradually with stirring and cooling, so that the temperature of the mixture was not allowed to reach 20 °C. Subsequently, the ice bath was removed and the flask was heated to 35 °C and maintained at this temperature for 30 min, followed by the slow addition of 92 mL of deionized (DI) water. The temperature of the reaction mixture increased to ca. 98 °C and the reaction vessel was maintained at this temperature for 15 min. Then, the suspension was further diluted with 280 mL of water and treated with 3% H_2O_2 until the cessation of gas evolution. Finally, the suspension was vacuum filtered and left to dry under a vacuum overnight after washing with copious amounts of DI H_2O. Power XRD of the prepared material was recorded on Bruker D8 Advance Diffractometer) using Cu K_α radiation. The morphologies of the sample were characterized with SEM (FE-SEM S-4800) and TEM (Joel JEM2010). The surface of as-prepared sample was characterized by Raman spectroscopy (LABRAM-1B) and FI-TR spectroscopy (NICOLET 6700). XPS was conducted with a Thermo Escalab 250 equipped with a hemispherical analyzer and using an aluminium anode as a source. Specific surface area of the sample was derived using the multipoint Braunauer-Emmett-Teller (BET) method. Power electronic conductivity investigation at the pressure of 4 MPa was performed on a Powder Resistivity Meter (FZ-2010, Changbao Analysis Co., Ltd, Shanghai, China).

Li-O_2 Battery Investigation: In the preparation of GO-based O_2 electrode, leaf-like GO (80 wt%) and a polyvinylidene fluoride binder (PVDF, 20 wt%) were intimately mixed in an *N*-methyl-2-pyrrolidone (NMP) solution, and the resulting slurry was coated on a carbon paper (TGP-H-060 carbon paper,[23] Torray). The total mass loading of leaf-like GO was 1 mg cm^{-2}. The coated electrode was dried for 12 h at 100 °C under vacuum to remove residual solvent. The batteries assembly was operated in a glove box filled with pure argon. The two electrodes are separated by a separator dipping with TEGDME–(1 M) $LiCF_3SO_3$ electrolyte.[23] This Li/separator/O_2 electrode was then sealed into a Swagelok cell with an air hole 0.8 cm^2 placed on the positive electrode side to allow the oxygen to flow in (Figure S5 in the Supporting Information). The cells were cycled in an LAND cycler Wuhan Land Electronic Co. Ltd. All experiments were carried out in a dry and pure oxygen glove box. In addition, conventional GO prepared by Hummers method, commercial CNTs (Nanotech Port Co., Ltd, Shenzhen, China), and their direct mixture (GO/CNTs weight ratio: 1:1) were also employed as the catalysts for Li-O_2 batteries. The

experiment conditions for these Li-O_2 batteries were the same as those for the leaf-like GO -based Li-O_2 battery. (Additional information about the Li-O_2 battery investigation is given in Figure S5, Supporting Information).

Li-Ion Battery Investigation: 70 mg nano-Si particles (40 nm Si powder; BET surface area: 115 $m^2 g^{-1}$; provided by the Center Research Institute of Chery Automobile Co., Ltd., China) were dispersed in ethanol (30 wt%) aqueous solution containing 30 mg leaf-like GO, and then the resulting solution was heated at 80 °C under stirring to vaporize the ethanol solution. Next, the as-prepared Si/GO mixture (90 wt%) was mixed with 5 wt% carbon black and 5 wt% polyvinylidene fluoride (PVDF), using NMP as the solvent, and then was spread on copper foil current collect to form a working electrode. Li metal foil was used as the anode, and 1 $LiPF_6$ dissolved in 1:1 v/v mixture of ethylene carbonate/diethyl carbonate (EC/DEC) was employed as the electrolyte. The mass loading of Si/GO mixture in working electrode is 4 mg cm^{-2}. Half cells (CR2016 coin-type) were fabricated to investigate the electrochemical behavior. The cell was cycled in an LAND cycler Wuhan Land Electronic Co. Ltd. (Additional information about the Li-ion battery investigation is given in Figure S6, in the Supporting Information).

EDLC Investigation: these electrodes were prepared by mixing 85 wt% leaf-like GO, 10 wt% conductive agent (carbon black) and 5 wt% poly(tetrafluoroethylene) (PTFE) binder dispersed in isopropanol. The slurries were rolled into a membrane and then pressed on the Al mesh current collectors. Thereafter, the electrodes were dried at 120 °C for 24 h in an oven. The typical mass loading of GO was about 2.6 mg cm^{-2}. A 1 M solution of tetraethylammonium tetrafluoroborate ($(C_2H_5)_4NBF_4$, $TEANBF_4$) dissolved in propylene carbonate (PC) was used as the electrolyte. The EDLC was assembled a glove box filled with pure argon. Two symmetric GO-based electrodes were separated by a separator dipping with $TEANBF_4$-PC electrolyte. This GO electrode/separator/GO-electrode was then sealed into a Swagelok cell to form an EDLC. CHI 660 was used for CV investigation. Additional information about the Li-ion battery investigation is given Figure S7 (Supporting Information).

Supporting Information

Supporting Information is available from the Wiley Online Library or from the author.

Acknowledgements

The authors acknowledge funding support from the National Natural Science Foundation of China (21103025, 20925312), the State Key Basic Research Program of PRC (2011CB935903), and Shanghai Science & Technology Committee (11DZ1100207,08DZ2270500). They also acknowledge Showa Giken Industrial Co., Ltd (Japan) and Chery Automobile Co., Ltd (China) for providing VGCF and nano-Si, respectively.

Received: January 12, 2013
Revised: February 1, 2013
Published online: April 9, 2013

[1] D. A. Dikin, S. Stankovich, E. J. Zimney, R. D. Piner, G. H. B. Dommett, G. Evmenenko, S. T. Nguyen, R. S. Ruoff, *Nature* **2007**, *448*, 457–460.
[2] S. Park, R. S. Ruoff, *Nat. Nanotechnol.* **2009**, *4*, 217–224.
[3] D. R. Dreyer, S. Park, C. W. Bielawski, R. S. Ruoff, *Chem. Soc. Rev.* **2010**, *39*, 228–240.
[4] G. Eda, G. Fanchini, M. Chhowalla, *Nat. Nanotechnol.* **2008**, *3*, 270–274.
[5] A. Bagri, C. Mattevi, M. Acik, Y. J. Chabal, M. Chhowalla, V. B. Shenoy, *Nat. Chem.* **2010**, *2*, 581–587.
[6] K. P. Loh, Q. L. Bao, G. Eda, M. Chhowalla, *Nat. Chem.* **2010**, *2*, 1015–1024.
[7] V. C. Tung, M. J. Allen, Y. Yang, R. B. Kaner, *Nat. Nanotechnol.* **2009**, *4*, 25–29.
[8] G. Eda, M. Chhowalla, *Adv. Mater.* **2010**, *22*, 2392–2415.
[9] W. Gao, L. B. Alemany, L. J. Ci, P. M. Ajayan, *Nat. Chem.* **2009**, *1*, 403–408.
[10] W. Gao, N. Singh, L. Song, Z. Liu, A. L. M. Reddy, L. J. Cui, R. Rajtai, Q. Zhang, B. Q. Wei, P. M. Ajayan, *Nat. Nanotechnol.* **2011**, *6*, 496–500.
[11] X. Wang, J. Zhi, K. Mullen, *Nano Lett.* **2008**, *8*, 323–327.
[12] H. A. Becerril, J. Mao, Z. Liu, R. M. Stoltenberg, Z. Bao, Y. Chen, *ACS Nano* **2008**, *2*, 463–470.
[13] G. Eda, C. Mattevi, H. Yamaguchi, H. Kim, M. Chhowalla, *J. Phys. Chem. C* **2009**, *113*, 15768–15771.
[14] C. Gómez-Navarro, J. C. Meyer, R. S. Sundaram, A. Chuvilin, S. Kurasch, M. Burghard, K. Kern, U. Kaiser, *Nano Lett.* **2010**, *10*, 1144–1148.
[15] W. S. Hummers, R. E. Offeman, *J. Am. Chem. Soc.* **1958**, *80*, 1339–1339.
[16] J. Qi, L. H. Jiang, Q. W. Tang, S. Zhu, S. L. Wang, B. L. Yi, G. Q. Sun, *Carbon* **2012**, *50*, 2824–2831.
[17] V. Lee, L. Whittaker, C. Jaye, K. M. Baroudi, D. A. Fischer, S. Banerjee, *Chem. Mater.* **2009**, *21*, 3905–3916.
[18] D. Graf, F. Molitor, K. Ensslin, C. Stampfer, A. Jungen, C. Hierold, L. Wirtz, *Nano Lett.* **2007**, *7*, 238–242.
[19] A. Ganguly, S. Sharma, P. Papakonstantinou, J. Hamilton, *J. Phys. Chem. C* **2011**, *115*, 17009–17019.
[20] Y. Si, E. T. Samulski, *Nano Lett.* **2008**, *8*, 1679–1682.
[21] J. I. Paredes, S. Villar-Rodil, A. Martinez-Alonso, J. M. D. Tascon, *Langmuir* **2008**, *24*, 10560–10564.
[22] S. F. Peng, H. M. Cheng, *Carbon*, **2012**, *50*, 3210–3228.
[23] H.G. Jung, J. Hassoun, J. B. Park, Y. K. Sun, B. Scrosati, *Nat. Chem.* **2012**, *4*, 579–585.
[24] Z. Q. Peng, S. A. Freunberger, Y. H. Chen, P. G. Bruce, *Science* **2012**, *337*, 563–566.
[25] P. G. Bruce, S. A. Freunberger, L. J. Hardwick, J. M. Tarascon, *Nat. Mater.* **2012**, *11*, 19–29.
[26] H. G. Jung, H. S. Kim, J. B. Park, I. H. Oh, J. Hassoun, C. S. Yoon, B. Scrosati, Y. K. Sun, *Nano Lett.* **2012**, *12*, 4333–4335.
[27] J. Xiao, D. H. Mei, X. L. Li, W. Xu, D. Wang, G. L. Graff, W. D. Bennett, Z. Nie, L. V. Saraf, I. A. Aksay, J. Liu, J. G. Zhang, *Nano Lett.* **2011**, *11*, 5071–5078.
[28] J. Hassoun, H. G. Jung, D. J. Lee, J. B. Park, K. Amine, Y. K. Sun, B. Scrosati, *Nano Lett.* **2012**, *12*, 5775–5779.
[29] A. Magasinski, P. Dixon, B. Hertzberg, A. Kvit, J. Ayala, G. Yushin, *Nat. Mater.* **2010**, *9*, 353–358.
[30] C. K. Chan, H. L. Peng, G. Liu, K. Mcllwrath, X. F. Zhang, R. A. Huggins, Y. Cui, *Nat. Nanotechnol.* **2008**, *3*, 31–35.
[31] I. Kovalenko, B. Zdyrko, A. Magasinski, B. Hertzberg, Z. Milicev, R. Burtovyy, L. Luzinov, G. Yushin, *Science* **2011**, *333*, 75–79.
[32] H. Wu, G. Chan, J. W. Choi, Y. Yao, M. T. McDowell, S. W. Lee, A. Jackson, Y. Yang, L. B. Hu, Y. Cui, *Nat. Nanotechnol.* **2012**, *7*, 309–314.
[33] P. Simon, Y. Gogotsi, *Nat. Mater.* **2008**, *7*, 845–854.
[34] S. Talapatra, S. Kar, R. Vajtai, L Cui, P. Victor, M. M. Shaijumon, S. Kaur, O. Nalamasu, P. M. Ajayan, *Nat. Nanotechnol.* **2006**, *1*, 112–116.
[35] H. J. Liu, J. Wang, C. X. Wang, Y. Y. Xia, *Adv. Energy Mater.* **2011**, *1*, 1101–1108.
[36] A. Izadi-Najafabadi, D. N. Futaba, S. Lijima, K. J. Hata, *J. Am. Chem. Soc.* **2010**, *132*, 18017–18019.
[37] H. Q. Li, R. L. Liu, D. Y. Zhao, Y. Y. Xia, *Carbon* **2007**, *45*, 2628–2635.
[38] H. J. Liu, X. M. Wang, W. J. Cui, Y. Q. Dou, D. Y. Zhao, Y. Y. Xia, *J. Mater. Chem.* **2010**, *20*, 4223–4230.
[39] T. Kyotani, *Carbon* **2000**, *38*, 269–286.